Non-destructive analysis of automotive paints with spectral domain optical coherence tomography

Yue Dong[1], Samuel Lawman[1, 2], Yalin Zheng[2], Dominic Williams[2], Jinke Zhang[1], Yao-Chun Shen[1*]

[1] *Department of Electrical Engineering & Electronics, University of Liverpool, United Kingdom, L69 3GJ*
[2]*Department of Eye and Vision Science, University of Liverpool, United Kingdom, L7 8TX*
[*]corresponding author: y.c.shen@liverpool.ac.uk

Reveived XX Month XXXX; revised XX Month, XXXX; accepted XX Month XXXX; posted XX Month XXXX (Doc. ID XXXXX); published XX Month XXXX.

We have demonstrated for the first time, to the best of our knowledge, the use of Optical Coherence Tomography (OCT) as an analytical tool for non-destructively characterizing the individual paint layer thickness of multiple layered automotive paints. A graph based segmentation method was used for automatical analysis of the thickness distribution for the top layers of solid color paints. The thicknesses measured with OCT were in a good agreement with the optical microscope and ultrasonic techniques that are the current standard in the automobile industry. Due to its high axial resolution (5.5 μm), the OCT technique was shown to be able to resolve the thickness of individual paint layers down to 11 μm. With its high lateral resolution (12.4 μm), the OCT system was also able to measure the cross sectional area of the aluminum flakes in a metallic automotive paint. The range of values measured was 300 to 1850 μm^2. In summary, the proposed OCT is a non-contact high resolution technique that has the potential for inclusion as part of the quality assurance process in automobile coating.

OCIS codes: *(120.0120) Instrumentation, measurement, and metrology; (120.4290) Non-destructive testing; (110.4500) Optical coherence tomography.*

http://dx.doi.org/10.1364/AO.??.????????

1. Introduction

The application of paint to a car body is a multi-stage process. The expensive auto body paint is usually applied in four coatings (Fig. 1): an electrocoat, a primer, a base coat and finally a clearcoat. The result of these successive paint layers is a surface that exhibits complex light interactions, giving the car a smooth, glossy and, if a metallic base coat, sparkly finish. More importantly, these paint layers not only provide appealing colour effects, but also have important functions such as corrosion prevention and waterproofing. It is hence of great interest to characterize car paint properties including thickness and uniformity for the purpose of quality control and quality assurance.

A number of techniques have been investigated as tools for the quality assurance of these coatings. In the automobile industry, the individual paint layer thickness is currently evaluated by ultrasonic testing method [1]. Ultrasonic testing is a contact technique and it only measures the thickness on a few numbers of sampling points. Hence it is short of enough information to detect localised paint defects and thickness distribution. Recently, terahertz (THz) pulsed imaging (TPI) has been demonstrated as a powerful technique for quantitatively characterizing individual paint layer thickness distribution and drying process non-destructively [2, 3, 4]. It has been shown that both the layer thickness and the refractive index can be determined by comparing the experimentally measured THz signal with the numerically simulated waveforms [3, 4]. However, the numerical fitting method is a computationally intensive process to accurately extract all eight parameters (four thicknesses and four refractive indices) from the measured THz signal. Both the measurement accuracy and the speed could be significantly improved with prior knowledge about one or more of the eight unknown parameters.

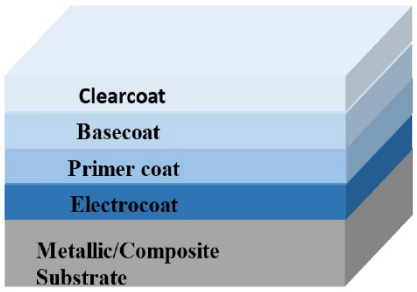

Figure 1. Schematic of a typical automotive paint sample with four paint layers including clearcoat, basecoat, primer coat and electrocoat, which applied on either metallic or composite substrate.

Optical coherence tomography (OCT) [5] is another non-destructive imaging technique that has better performance in both axial and lateral resolutions. OCT has become a standard diagnostic instrument in ophthalmological diagnosis [6]. Recently OCT has also found uses in many non-medical fields [7], including thickness measurement of paper [8], fluttering foils [9], and pharmaceutical tablet coating [10, 11]. In this paper, we demonstrate for the first time that the spectral domain OCT (SD-OCT) [12] can be used to assess the top two layers of real-world automotive paints. While OCT has already been demonstrated as an effective tool for imaging paint layers and underdrawings of museum paintings [13-16], the complex and unknown structure of these objects generally requires skilled human qualitative assessment input to interpret. The application of OCT to quality control for automotive paints is quite different in the required output. The system needs to automatically return quantitative paint layers structural information. To achieve this automatic output, in this paper we firstly apply image segmentation to quantitatively evaluate not only the overall paint layers thickness but also the thickness distribution and uniformity of the whole area under measurement. Secondly we use thresholding to recover the locations and sizes of metallic flakes within a paint layer. Owing to the relative shorter wavelength and broadband nature of the light source, SD-OCT shows to be able to measure with high precision the layer thickness of the top paint layers in the range from 11 μm to 100 μm without any numerically fitting method. Great consistency is shown between the results of SD-OCT measurements and two other reference techniques, ultrasonic testing and optical microscope. Moreover, the density (number of flakes per unit area) and dimensions of aluminium flakes in the basecoat layer of a metallic coloured paint sample are also determined using the SD-OCT system. These are the most important parameters for the sparkle effect of the automotive paints, which are not able to be determined by any other active industry benchmarks techniques.

2. Method and Materials

A. SD-OCT system and performance

All OCT measurements presented in this paper were performed by an in-house SD-OCT system [17]. Fig. 2 shows its schematic diagram. A superluminescent diode light source (EXLOAS EXS210040-01) was used. The centre wavelength is 840 nm and the spectral full width at half maximum (FWHM) is 47 nm. The collimated light beam was divided into a reference and a sample beams using a broadband 50:50 beam splitter. Then the back-scattered light from the sample was collected using an achromatic lens and the collected light was subsequently recombined with the back reflected light from the reference reflector. The resultant spectral interferogram was recorded using a high-resolution spectrometer (HR2000+, Ocean Optics).

Theoretically the spectral interferogram I(λ) between the sample and reference reflector can be expressed by:

$$I(\lambda)=S(\lambda)[R_r+\sum_1^N R_n + 2\sum_{m\neq n}\sqrt{R_m R_n}\cos(2\pi\Delta z_{mn}/\lambda) + 2\sum_1^N \sqrt{R_r R_n}\cos(2\pi\Delta z_n/\lambda)] \quad (1)$$

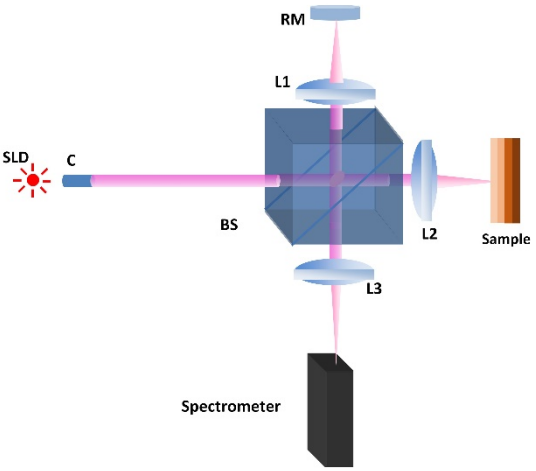

Figure 2. Schematic diagram of the in-house SD-OCT system. BS: beam splitter; L1, L2, L3: achromatic lenses; C: collimator; RM: reference mirror.

where S(λ) is the spectral power density of the light source; Rr and Rn are the reflectivity of the reference reflector and the n-th sample interface respectively; λ is the wavelength and Δz_{nm} and Δz_n denotes the optical path length difference (OPD) between sample interfaces n and m, and the reference reflector and sample interface n, respectively. Eq. (1) contains four terms. The first two terms are the DC component, which produces a strong signal at the zero OPD position. The second term is the auto-correlation between the different interfaces of the sample, which can produce unwanted image ghosts. The last term, which contains the desired sample structure information, is the cross-correlation between the reference reflector and the sample interfaces. Apart from the cross-correlation term, the other three terms will contaminate the final OCT cross-sectional image. In order to minimize the contamination introduced by the mutual correlation component, the reference reflected light intensity can be set much stronger than the back-scattered sample beam (Rr>>Rn). Alternatively, by taking two separate spectral interferograms with a phase shift of π on the same sampling point, the DC and mutual correlation components can be completely removed in their differential interferogram [18].

The recorded discrete spectral interferogram I(λ) is firstly interpolated into equal wavenumber spacing, I(k). It is then zero padded before applying a Fast Fourier Transform (FFT) algorithm to generate the depth profile. Assuming the DC and auto-correlation terms are removed by the above-mentioned phase shift method, the OCT depth profile (A-scan) can be expressed as:

$$R(z) = DFT\{I(k)\} = DFT\{S(k)\}\otimes[2\sum_1^N \sqrt{R_r R_n}\,\delta(z\pm\Delta z_n)] \quad (2)$$

where ⊗ stands for convolution and δ stands for Kroneka Delta function. The theoretical axial resolution is determined by the FWHM of the axial point spread function (PSF), which is given by Fourier transforming of the power spectral density of the light source. To experimentally measure the axial resolution, we took the FWHM of the main peak in the depth profiles. The

blue curve in Fig. 3 (a) shows the spectral interferogram between a glass plate and a reference reflector. After the data interpolation, zero padding and FFT, the depth profile is generated and shown by the blue waveform in Fig. 3(b). The sharp cut off of the spectrum at 800 nm due to the range of the spectrometer used introduces additional ringing (side lobe) artefacts. These are removed by applying a Tukey window before the FFT. The red waveform shown in Fig.3 (b) is the OCT depth profile generated by first applying a Tukey window function on the original measurement spectral interferogram. The window function has no significant effect on the axial resolution but reduces the side lobes significantly. The axial resolution determined by the FWHM of the main peak in the depth profile is 5.5 μm in air which is significantly better than the typical value for TPI (30 μm) method.

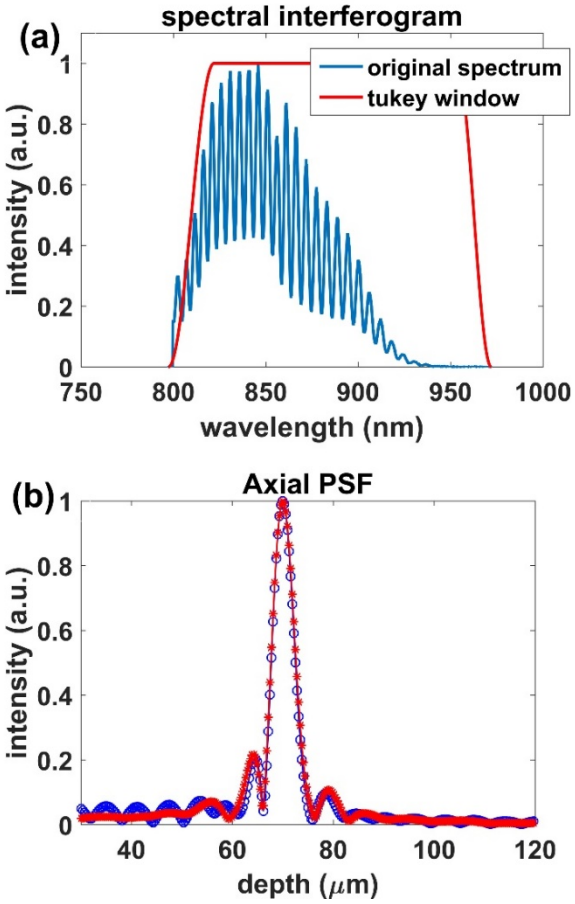

Figure 3. (a)Blue – spectral interferogram between glass and reference mirror. Red – tukey window function applied on the spectral interferogram to reduce the side lobes in the depth profile. (b) Depth profiles extracted from the original (blue) and windowed (red) spectral interferogram.

In order to determine the lateral resolution of the SD-OCT system, the USAF 1951 resolution target (Thorlabs, Germany) was scanned. As shown in Fig. 4, the smallest bars that the SD-OCT system cannot resolve on the resolution target are the 3rd elements of the 6th bar group. This corresponds to a lateral resolution of about 12.4 μm.

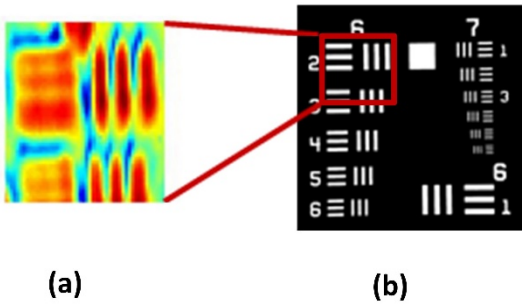

Figure 4. The (a) OCT enface image of the 2nd and 3rd elements in the sixth bar group of (b) USAF 1951 resolution target measured by the SD-OCT system.

B. Automobile paint samples

In this study, automotive paint samples with four different basecoats were measured. The first three sets are solid colour automotive samples with white, black and onyx basecoats respectively. These three paint samples are non-metallic. The fourth set of paint sample is a silver metallic colour sample, which has sparkle effect due to aluminium flakes in the basecoat layer. Each set consists of two individual paint samples. One applied on metal substrate and the other one applied on carbon fibre composite material substrate that is increasingly being used in the automobile industry due to its stiffness and lightweight nature. As shown in Fig. 1, all of these samples were prepared with four layers to be representative of real-world automotive paint layer structures. The individual thickness of each paint layer is typically ranges from 10 μm to 100 μm depending on different function of each layer. The total thickness of all the four layers is in the range from 170 μm to 240 μm.

3. Results and Discussion

A. Solid colour paint samples

In each experiment, the OCT took one B-scan consists of 200 A-scans over a lateral range of 1 mm. Hence the distance between each A-Scan is 5 μm. Fig. 5 shows the typical cross-sectional images of the solid colour samples.

The light penetration depth in the sample depends on the scattering and absorption properties of different layers. For all samples the transparent clearcoat can be seen in their cross-sectional image due to the low scattering and low absorption of this pigment free paint layer. For the black and onyx basecoat samples shown in Fig. 5(a) and Fig. 5(b), the basecoats appear almost as transparent as their clearcoats. The absorption and scattering of the NIR light by these pigmented basecoat layers are not sufficient to stop the OCT from being able to see through them. Below the basecoat layers, the highly absorbing primer coat absorbs most of the incident light, hence neither of the primer coat nor electrocoat could be resolved by the OCT system in this wavelength region (850 nm). The cross-sectional image of the white basecoat sample shown in Fig. 5(c) demonstrates that it has a transparent clearcoat layer as well. However, different from the black and onyx samples, the strongly multiple scattering property of the titanium dioxide in the white basecoat limits the penetration depth of the incident light [19]. Light entering this layer is scattered many times within a short distance, meaning no structure underneath it can be resolved. So far, for non-metallic paints, this only appears to

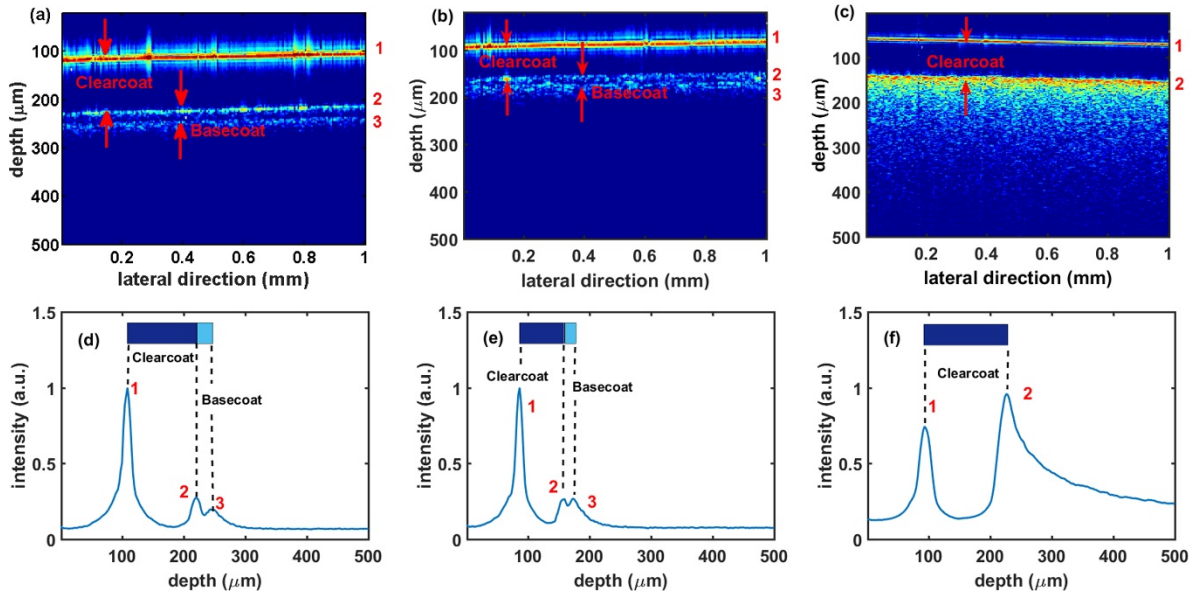

Figure 5. OCT cross-sectional images of automotive paint samples with (a) black, (b) onyx, (c) white basecoat. Averaged depth profile of automotive paint samples with (d) black, (e) onyx, and (f) white basecoat. 1 – surface; 2 – clearcoat/basecoat interface; 3 – basecoat/primer coat interface. All the solid colour samples have transparent clearcoat. The basecoat of black and onyx samples are transparent as well but the white basecoat is cloudy due to the strongly scattering of the titanium dioxide.

be an issue with white or near white basecoats with high titanium dioxide content. One method of increasing penetration in the white and highly reflective base coats is to select a wavelength of light where these are more transparent. Recently both the time-domain and Fourier-domain OCT have been developed that uses 1960 nm infra-red light [20, 21], where titanium dioxide white paint layers have been shown to be transparent. [20].

The coating thickness of each paint layer is one of the most important parameters for characterising the painting quality in automobile industry. Ideally, the individual coating thickness of a sampling point can be determined by finding the interface peaks in the OCT depth profile. In practice, it is actually difficult to distinguish the interface peaks with pigment-introduced peaks in a single OCT depth profile. By averaging the neighbouring depth profiles of a sample, the interface peaks will be significantly enhanced as shown in Fig. 5(d) - (f). The average thickness of each paint layer can be worked out by the distance between the boundaries of each layer divided by their refractive indices [3] (1.56 for clearcoat and 1.64 for basecoat) respectively. However, the averaging of depth profiles/a-scans loses spatial information useful to access the distribution **and** uniformity of an individual paint layer.

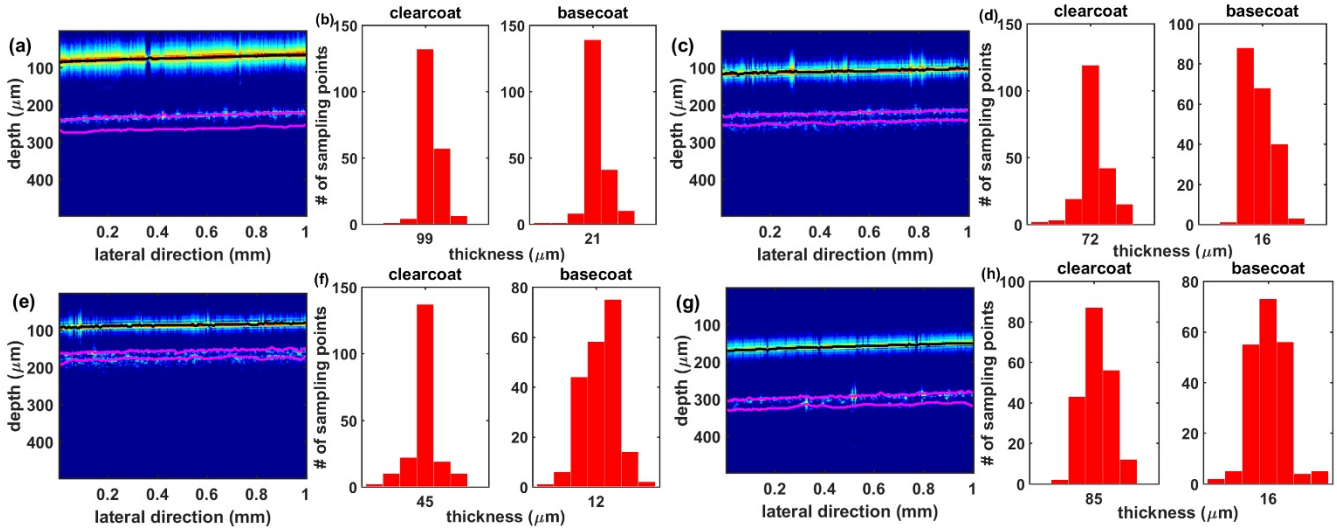

Figure 6. Thickness distribution information of solid colour automotive paint samples. Top raw: black; bottom raw: onyx. (a) (c) (e) (g) – surface and interfaces of extracted by graphic segmentation; black – surface; pink - interfaces. (b) (d) (f) (h) Thickness distribution of clearcoat and basecoat.

Table 1. Individual paint thickness (μm) measured by SD-OCT, ultrasonic testing and optical microscope

	Clearcoat		Validation		Basecoat		Validation	
	Mean	Std	Ultrasonic	Optical	Mean	Std	Ultrasonic	Optical
Black A	99.8	1.33	102.4	103.3	20.9	1.71	19.8	20.6
Black B	72.3	1.58	74.9	74.4	15.3	1.45	15.2	14.7
Onyx A	44.6	1.81	45.7	45.5	11.8	2.1	11.4	12.2
Onyx B	85.5	1.46	87.4	87.9	15.4	2.43	17.5	18.0

In this study, a graph based segmentation algorithm was used to detect the position of surface and interfaces on all sampling points in an OCT cross-sectional B scan image [22]. More specifically, the image is represented as a graph whereas each pixel of the image is regarded as a node of the graph. Now the surface / interface segmentation problem becomes to find the shortest path from the left to the right of the image according to an energy functional as defined by the gradient information of the image. The surface and interfaces will be detected one by one by repeatedly applying this segmentation approach. Hence the coating thickness of all the sampling points can be worked out rather than an averaging value. As shown in Fig. 6, the black and pink lines in the images stand for the extracted surfaces and interfaces respectively. The clearcoat and basecoat thickness distribution of the solid colour paint samples were calculated by the distance between the extracted surface and interfaces and shown in the histograms at the right hand sides of their corresponding images. The thinnest resolved basecoat thickness is 11.8 μm. Furthermore, our OCT method also provides the standard deviations of each paint layer which can be used to evaluate its uniformity.

In order to validate the OCT measured thickness, two currently used reference techniques, optical microscope and ultrasonic (μP501A PELT multi-layer thickness gauge) testing, were applied independently on the samples to measure the thickness of individual paint layers. The mean OCT measured thicknesses, and the optical and ultrasonic measured thicknesses are listed in Table 1 for comparison. The OCT measured thickness shows a good agreement with the reference techniques. The maximum difference between the OCT measured thickness and the two reference techniques is less than 3.5 μm.

B. Metallic basecoat paint samples

The effect of sparkly finish of an automotive paint lie on the dimensions and the orientations of the aluminium flakes in the metallic basecoat layer. In order to characterise the dimensions of the aluminium flakes in the metallic basecoat paint samples, a lateral area of 1 mm x 0.1 mm scanned with the OCT. As shown in Fig. 7 (a), ten B-scans were taken in this area and the distance between each B-scan was 10 μm. For each B-scan, OCT measured 200 spectral interferograms (A-Scans) covering a length of 1 mm that is the same as the solid basecoat samples. Fig. 7(b) shows the cross-sectional image generated from one of the measured B-scan data sets. As discussed above, the clearcoat is transparent. In the basecoat, there are high intensity reflections from the aluminium flakes. This high reflectance causes an image artefact, due to the multiple reflections between the flakes and surface of the clearcoat, to be visible under the basecoat in the cross-sectional image. Fig. 7(c) shows the peak intensity map of the basecoat. High intensity corresponds to reflection from flakes. In order to determine the boundary of the aluminium flakes, the simplest image method, namely thresholding, was applied on the intensity map. The thresholding parameter used in this work is an empirical value. Pixels located at the boundaries of clearly distinguished flakes were manually selected. The mean intensity of these boundary pixels was subsequently used as the thresholding parameter. After thresholding, 15 flakes were detected and are shown in Fig. 7(d). By counting the pixels for selected flakes, the biggest flake in the area contains 37 pixels

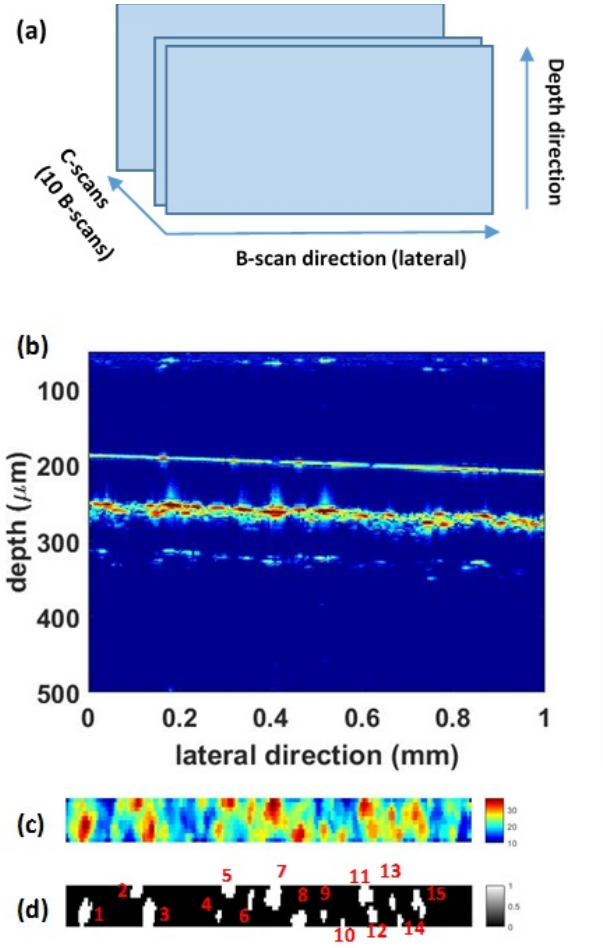

Figure 7 (a) OCT scanning scheme for the metallic basecoat paint sample. (b) OCT cross-sectional image. (c) 2-D peak intensity map of the metallic basecoat. (d) Fifteen selected aluminium flakes by thresholding.

that equivalent to 1850 μm² and the smallest one contains 6 pixels equivalent to 300 μm². The mean area for the flakes is 930 μm². Therefore the OCT technique reported here may provide an unique way for determining the size and orientation of the metal flakes within the automobile coatings. To the best of our knowledge, there is currently no other techniques capable of doing this.

4. Conclusion

Firstly, SD-OCT is a new method to measure the upper layer thicknesses of automobile paints. The thickness of the clearcoat is always resolvable. For non-metallic and non-white samples the thickness of the basecoat is also resolvable. The range of layer thicknesses resolved was 11.8 to 100 μm. The OCT thickness measurements were consistent with those measured by ultrasound and optical microscopy. Furthermore, because of its high spatial resolution OCT is able to provide the thickness distribution and uniformity information for each individual layers of the car paints.

Automobile coating quality assurance is a new application for OCT. The technique has benefits over current methods, such as being non-contact and providing far more spatial information. It may also complement other new methods, such as Terahertz imaging.

Acknowledgments: The authors would like to thank Dr. Su and Dr. Zeitler of Cambridge University for helpful discussions . This work is supported by UK EPSRC Research Grant EP/L019787/1 and EP/K023349/1.

References:

1. M. X. Li, X. M. Wang, and J. Mao, "Thickness measurement of a film on a substrate by low-frequency ultrasound," Chin. Phys. Lett. **21,** 870-873 (2004).
2. T. Yasui, T. Yasuda, K. Sawanaka, and T. Araki, "Terahertz paintmeter for noncontact monitoring of thickness and drying progress in paint film," Appl. Opt. **44**, 6849–6856 (2005).
3. K. Su, Y. C. Shen, J. A. Zeitler, "Terahertz sensor for non-contact thickness and quality measurement of automobile paints of varying complexity," IEEE. Trans. THz Sci. Technol. **4**, 432-439 (2014).
4. T. Yasuda, T. Iwata, T. Araki, and T. Yasui, "Improvement of minimum paint film thickness for THz paint meters by multiple-regression analysis," Appl. Opt. **46**, 7518–7526 (2007).
5. D. Huang, E. A. Swanson, C. P. Lin, J. S. Schuman, W. G. Stinson, W. Chang, M. R. Hee, T. Flotte, K. Gregory, C. A. Puliafito, et al, "Optical coherence tomography," Science **254**, 1178-1181 (1991).
6. S. Marschall, B. Sander, M. Mogensen, T. M. Jorgensen, P. E. Andersen, "Optical coherence tomography – current technology and applications in clinical and biomedical research," Anal. Bioanal. Chem. **400**, 2699-2720 (2011).
7. D. Stifter, "Beyond biomedicine: a review of alternative applications and developments for optical coherence tomography," Appl. Phys. B **88**, 337-357 (2007).
8. T. Fabritius, E. Alarousu, T. Prykari, J. Hast, R. Myllyla. "Characterisation of optically cleared paper by optical coherence tomography," Quantum Electron **36**, 181-187 (2006).
9. A. Nemeth, R. Gahleitner, G. Hannesschlager, G. Pfandler, M. Leitner, "Ambiguity-free spectral-domain optical coherence tomography for determining the layer thicknesses in fluttering foils in real time," Opt. Laser Eng. **50**, 1372-1376 (2012).
10. S. Zhong, Y. C. Shen, L. Ho, R. K. May, J. A. Zeitler, M. Evans, P. F. Taday, M. Pepper, T. Rades, K. C. Gordon, R. Muller, P. Kleinebudde, "Non-destructive quantification of pharmaceutical tablet coatings using terahertz pulsed imaging and optical coherence tomography," Opt. Laser Eng. **49**, 361-365 (2011).
11. D. M. Koller, G. Hannesschlager, M. Leitner, J. G. Khinast, "Non-destructive analysis of tablet coatings with optical coherence tomography," Eur. J. Pharm. Sci. **44**, 142-148 (2011).
12. G. Hausler and M.W. Lindner, "Coherence Radar and spectral radar –new tool for dermatological diagnosis," J. Biomed. Opt. **3**, 21 -31 (1998).
13. H. Liang, M. G. Cid, R.G. Cucu, G. M. Dobre, A. Podoleanu, J. Pedro, and D. Saunders, "En-face Optical Coherence Tomography – a novel application of non-invasive imaging to art conservation," Opt. Express **13**, 6133-6144 (2005).
14. C. S. Cheung, M. Spring, and H. Liang, "Ultra-high resolution Fourier domain optical coherence tomography for old master paintings," Opt. Express **23**, 10145-10157 (2015).
15. P. Targowski, R. Ostrowski, M. Marczak, M. Sylwestrzak, and E. A. Kwiatkowska, "Picosecond laser ablation system with process control by optical coherence tomography," Proc. SPIE 7391, 73910G (2009).
16. P. Targowski, M. Góra, T. Bajraszewski, M. Szkulmowski, B. Rouba, T. Łękawa-Wysłouch, and L. Tymińska-Widmer, "Optical coherence tomography for tracking canvas deformation," Laser Chem. 2006, 93658 (2006).
17. H. Lin, Y. Dong, Y. C. Shen and J. A. Zeitler, "Quantifying pharmaceutical film coating with optical coherence tomography and terahertz pulsed imaging: an evaluation," J Pharm Sci. **104**, 3377–3385 (2015).
18. Z. H. Ma, R. K. Wang, F. Zhang, J. Q. Yao, "Spectral optical coherence tomography using two-phase shifting method," Chin. Phys. Lett. **22**, 1909–1912 (2005).
19. H. Liang, R. Lange, B. Peric, M. Spring, "Optimum spectral window for imaging of art with optical coherence tomography," Appl. Phys. B **111**, 589-602 (2013).
20. C. S. Cheung, J. M. O. Daniels, M. Tokurakawa, W. A. Clarkson Wa, and H, Liang, "Optical coherence tomography in the two-micron wavelength regime for paint and other high opacity material," Opt. Lett. **39**, 6509-6512 (2014).
21. C. S. Cheung, J. M. O. Daniels, M. Tokurakawa, W.A. Clarkson Wa, and H. Liang, "High resolution Fourier domain optical coherence tomography in the 2 μm wavelength range using a broadband supercontinuum source," Opt. Express **23**, 1992-2001 (2015).
22. D. Williams, Y. Zheng, P. G. Davey, F. Bao, M. Shen, and A. Elsheikh, "Reconstruction of 3D surface maps from anterior segment optical coherence tomography images using graph theory and genetic algorithms," Biomed. Signal Process Control **25**, 91-98 (2016).